Applicability of Theoretical Optimal Pulse to the Thoracic Response of the Human Body Finite Element Model during Frontal Impact

Yasuki Motozawa, Yuichi Ito, Fumie Mori

Abstract The present paper describes an analysis regarding effects of the theoretical vehicle pulses optimized for an anthropomorphic test device (ATD) on the human body during frontal crashes. In previous studies, the authors derived theoretical pulses using a transfer function of a one-dimensional model. The effectiveness of those pulses had successfully been validated on ATD by a multi-body simulation and an experiment. However, it had not been examined as to whether or not the optimal pulses are effective on the human body as well. In the present study, the authors applied the theoretical optimal pulse and rectilinear pulse to human and ATD finite element (FE) models. The human FE models used represent the property of 50th percentile American males aged 35 and 75 years old (Y/O). The thoracic response of those models was analyzed. When applying the theoretical pulses to the human models, the thoracic deflection indicated linear increase along the time axis after onset. The human model aged 75 Y/O indicated larger deflection than the model aged 35 Y/O due to plastic deformation of the rib cage. The results indicated that the thoracic deflection is sensitive to the duration of the applied pulse in the human models.

Keywords finite element, human model, optimization, thoracic response, vehicle pulse

I. INTRODUCTION

Recently, age-related injury, especially rib fracture during vehicle impact, has become a social issue. Acceleration-based injury indices measured by ATD have been widely applied to the evaluation as the indices to represent “global” injury severity. However, there have been many discussions regarding more appropriate indices that enable quantitative prediction of injury of actual humans, such as the probability of rib fracture. Among them, the maximum value of thoracic deflection is currently regarded as one of the possibilities. Therefore, an approach to the theoretical optimization of a restraint system for those indices should be an issue worthy of investigation.

It has been reported that the boundary condition between the thorax and the restraint system, i.e. load distribution along the contact area, can contribute to the thoracic deflection or rib fracture [1-2]. However, load distribution along the time domain, or optimization of the time history of applied force, has not been examined systematically with regard to thoracic deflection. It is known that the time history of vehicle deceleration, i.e. crash pulse, affects the occupant injury indices such as the maximum value of the thoracic deceleration [3-5]. From the early era of automotive safety technology, a number of attempts were made to optimize deceleration pulse during a crash by a sensitivity analysis, or a simpler “cut and try” method [4-5]. Numerical simulation was also done as well as experimental optimization to determine a better pulse [5]. In those studies it was found that the optimized pulses that minimize the peak value of the occupant deceleration have identical characteristics in shape. They consist of three segments of the magnitude of deceleration along the time domain during impacts [5]. In their previous studies, by using a single degree of freedom (SDOF) model, the authors theoretically derived optimal pulses that feature identical characteristics in shape to those of pulses experimentally optimized. They also successfully validated their effectiveness to the thoracic deceleration by using ATD experiments as well as three-dimensional multi-body computational model simulations [6-7].

However, to the authors’ best knowledge, those optimizations were done only to the response of the ATD, and the applicability of those pulses to the human response had not been reported. The aim of the present study is to examine the applicability of those classic theoretical optimal pulses to human occupants. The

Yasuki Motozawa is Chief Engineer of Honda R&D Co., Ltd. Automobile R&D Center in Japan (e-mail: yasuki_motozawa@n.t.rd.honda.co.jp). Yuichi Ito is Engineer of Honda R&D Co., Ltd. Fumie Mori is Engineer of PSG Co. Ltd. in Japan.

authors applied the theoretical optimal pulses, as well as rectilinear pulse, to the simulated sled-buck, accommodating human or ATD FE models. The human FE models used in the present study represent the anthropometry and material property of 50th percentile American males of ages 35 and 75 years. The thoracic response of those models was analyzed.

II. METHODS

Theoretical optimal pulse

In their previous studies, the authors conducted theoretical studies regarding optimal pulse during a frontal vehicle impact by using a SDOF model [6].

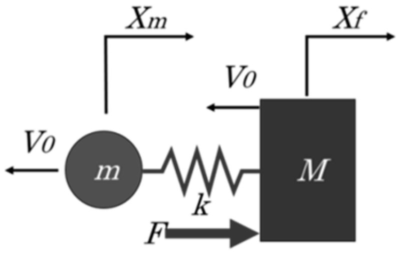

Fig. 1. SDOF model used in the previous studies

Figure 1 indicates the SDOF model used in their previous studies. The system for the thorax of the occupant, vehicle and restraint system can be modeled as indicated in Figure 1, with the thorax of the occupant as a lumped mass of m, the vehicle as a lumped mass of M and the restraint system as a linear spring with a spring coefficient of k. To manage the initial kinetic energy of the occupants during an impact with the minimum thoracic deceleration, the value of occupants' (thoracic) deceleration $\ddot{X}_m$ should be constant throughout the time domain; i.e., a rectilinear pulse. The authors determined a target pulse for $\ddot{X}_m$ that approximates a rectilinear pulse with the least difference, satisfying the initial conditions of the constraint of a linear spring SDOF model. Figure 2 indicates a schematic target pulse for $\ddot{X}_m$. Where, the target value of the maximum thoracic deceleration $\ddot{X}_m$ is denoted as C.

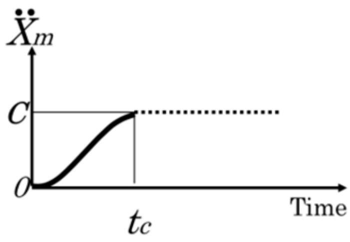

Fig. 2. Schematic target pulse for $\ddot{X}_m$

The pulse for $\ddot{X}_m$ is segmented into two phases along the time domain. The authors denoted the time where the pulse is segmented as the control time t_c. Then the authors derived the following theoretical optimal vehicle deceleration pulses for $\ddot{X}_f$, by using inverse Laplace transform of the target waveforms.

$$\ddot{X}_f = \left(\frac{\gamma}{\pi}\right)^3 \left\{\left(2t - 3\frac{\pi}{\gamma}\right)t^2 + \frac{6}{\omega^2}\left(2t - \frac{\pi}{\gamma}\right)\right\} \qquad \text{[Polynomial-type]} \qquad (1)$$

$$\ddot{X}_f = \frac{C}{2}\left\{1 + \left(\frac{\gamma^2}{\omega^2} - 1\right)\cos\gamma t\right\} \qquad \text{[Cosine-type]} \qquad (2)$$

$$\ddot{X}_f = C\frac{\gamma}{\pi}\left\{t + \left(\frac{4\gamma^2}{\omega^2} - 1\right)\frac{1}{2\gamma}\sin 2\gamma t\right\} \qquad \text{[Sine-type]} \qquad (3)$$

Where, $\omega = \sqrt{\frac{k}{m}}$, $\gamma = \pi/t_c$

These are the representative function forms of the theoretical optimal pulse. The curves for these pulses are shown in Figure 3. Although they indicate different waveforms according to each function form, they have identical characteristics in shape as described in the above paragraph.

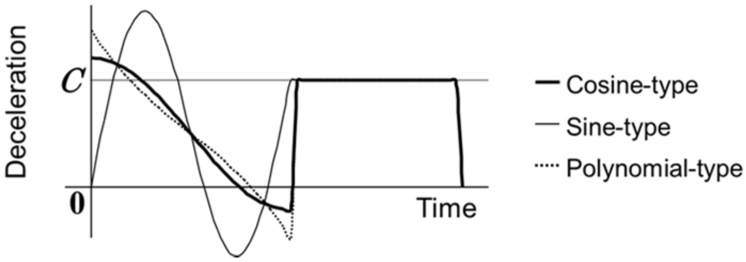

Fig. 3. Representative theoretical optimal pulse

Throughout the previous studies including those of the authors, identifications for SDOF models were performed using an ATD rather than a human body. Moreover, those identifications are based on a number of suppositions, i.e., radical simplifications. The equivalent mass representing the mass of the thorax is regarded as a constant value. This means that the contribution of the kinematics of the other body regions is omitted throughout the impact. The spring coefficient representing the stiffness of the restraint system and the thorax is regarded as a constant in the same manner. This means the non-linearity due to rate dependency or elastoplasticity of the human tissue is regarded as negligible. Wu et al. addressed the limitations of linear spring models and they attempted to describe more generic optimization considering non-linearity of the restraint system [8]. However, since they mainly focused on the response of the ATD rather than that of humans, they did not address the non-linearity of the human body. Moreover, they had not practically validated the applicability of their optimization against either ATD or human subjects. Therefore, in the present study the authors conducted the FE simulation using both human models and ATD and compared their thoracic responses.

FE Simulation Models

The human FE models used in the present study, established by Ito et al. [9-11] and Dokko et al. [12-13], represent the anthropometry and material properties of 50th percentile American males aged 35 and 75 years old (hereafter, Y/O). The human FE models incorporated the lower limbs, lumbar spine and thorax models previously developed by Ito et al. [9-11] and Dokko et al. [12-13]. The remaining body regions, i.e., the head/neck and the upper extremities, were supplemented by the H-Model™, which is a commercially available generic human body FE model consisting of 304,390 elements [14]. Figure 4 indicates the perspective view of the adult FE model, along with the geometry of the rib cage in the adult and elderly models.

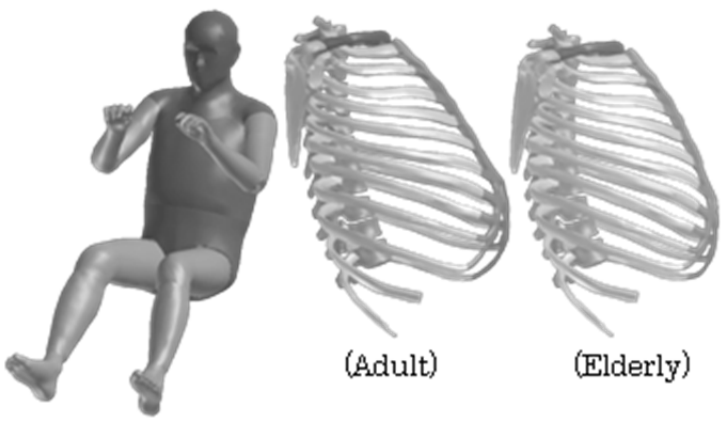

Fig. 4. Perspective view of adult FE model, along with geometry of rib cage in adult and elderly models

The range of the values for the material parameters, the Young's modulus, yield stress, ultimate stress and strain of the femur, tibia, fibula, lumbar spine, clavicle, rib and sternum, were determined by Ito et al. [9-11] and Dokko et al. [12-13] from the literature previously published [15-16]. PAM-CRASH™ was used as the FEM solver. Ito et al. [9-11] validated the response of the thoracic component of both human FE models during a pendulum impact against the results of published experiment performed by Kroell et al. [17-18]. They also validated the responses during a table-top thoracic belt loading against the experiments performed by Lessley et al. [19]. The authors [20] evaluated the differences between the simulation and the experiments using a ranking system to assess the biofidelity of the model according to the methodology proposed by Rhule et al. [15]. They compared the time histories of the displacement of the head, vertebral bodies and pelvis of the adult human FE model to the averages of the sled experiments. Consequently, they successfully validated sufficient biofidelity of the model during frontal impacts.

In the present study, an ATD FE model (hereafter, dummy FE model) developed by FTSS was used for comparison with a human FE model. The dummy FE model represents the Hybrid III AM50th percentile anthropometric dummy. The thoracic response of the model during a pendulum impact was validated against the results of published experiment performed by Kroell et al. [17-18] as well.

The authors developed a sled-buck FE model (hereafter sled-buck model). The model represents the fundamental geometry of a small-size sedan-type vehicle, consisting of a floor panel, a front seat and a set of seatbelts. The floor panel was modeled as a shell element. The seatbelts were modeled using bar and membrane elements in which force-elongation properties of the actual material of the webbing used in the small-size production vehicle were reflected. The cushion of the front seat was modeled as a solid element. However, an instrument panel, steering wheel and column assembly, seatbelt pre-tensioner, load-limiter and airbag were omitted (Figure 5).

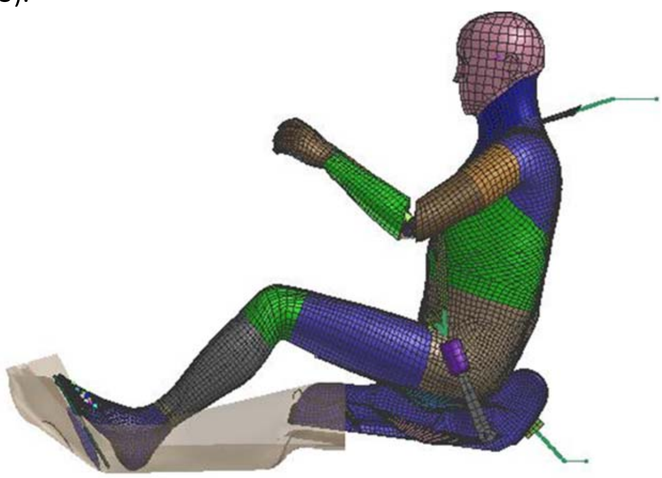

Fig. 5. Adult human FE model in sled-buck model representing interior of small-size sedan-type vehicle

Phase 1 Simulations: Response to Rectilinear Pulse

In the first phase, the authors applied a number of rectilinear deceleration pulses to the sled-buck model, accommodating the adult and elderly human FE models and the dummy FE model, to identify the natural frequency of the systemω. First, they applied rectilinear pulses with different magnitudes and with an identical duration of 71 ms to the models (Table I). Then, they applied pulses with different durations and with an identical magnitude of 22.7 G to the models as well (Table II).

TABLE I
RECTILINEAR PULSES APPLIED TO THE SLED-BUCK MODEL WITH IDENTICAL DURATION

Magnitude (G)	Duration (ms)	Delta V (km/s)
22.7	71	56
19.5	71	48
16.2	71	40
13.0	71	32
9.73	71	24
6.49	71	16

TABLE II
RECTILINEAR PULSES APPLIED TO THE SLED-BUCK MODEL WITH IDENTICAL MAGNITUDE

Magnitude (G)	Duration (ms)	Delta V (km/s)
(22.7)	(71)	(56)
22.7	61	48
22.7	51	40
22.7	41	32
22.7	30	24

The time histories (hereafter pulses) of the thoracic deceleration and deflection were measured. For the human FE models, T8 was defined as a reference point for the thoracic deceleration by comparing the geometry of the thoracic rib cage of the human model to the dummy. The distance from the sternum to T8 was defined as the thoracic deflection of the human FE models. In the dummy model used in the present study, the distance from the sternum to the thoracic spine is defined as the thoracic deflection.

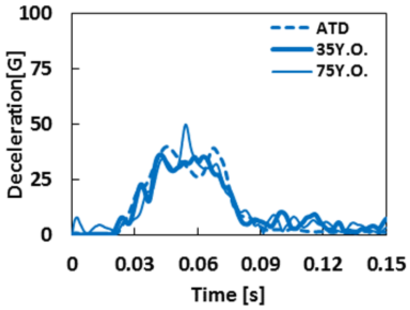

Fig. 6. Thoracic deceleration pulses for input pulse with magnitude of 16.2G and duration of 71 ms

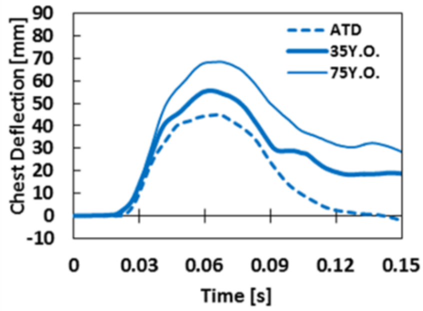

Fig. 7. Thoracic deflection pulses for input pulse with magnitude of 16.2G and duration of 71 ms

Figures 6 and 7 indicate representative thoracic deceleration and deflection pulses. They are for the applied pulse with magnitude of 16.2 G and duration of 71 ms. The pulses of the thoracic deceleration in the dummy and those of the human models indicated similar trends, but in the human models it is difficult to identify the rise time (π/ω) of each pulse from their shapes due to the vibration.

The theoretical optimal pulses determined by Equations 1, 2 and 3 are based on the supposition that the equivalent mass and the spring coefficient were constant. Under those suppositions, the chest deflection should always be proportional to the chest deceleration. From Figure 7, it is observed that the shapes of the thoracic deflection pulses indicate approximately haversine response during the onset in both the human models and the dummy model. With higher (16.2 G or over) magnitudes of applied pulse, the rise time is approximately identical among models (Figures from 20 to 32 in Appendix). Therefore, the authors identified 60ms of the rise time from the pulses of the thoracic deflection as well as those of deceleration. Thus, the natural frequency of the system ω was identified as 52.7 rad/s.

Phase 2 Simulations: Response to Theoretical Optimal Pulse

Based on the results of Phase 1 simulations, the authors determined the theoretical optimal pulses to be applied to the models. Among the representative function forms as indicated above, they selected cosine-type function form described by Equation 2. This is because it is the mathematically simplest and with the smallest intensity (range of peak-to-peak value) for an identical control timet_c, which is deemed to be the most appropriate waveform among them as a reference.

In Equation 2, γ and C may be set to any value. The authors determined an initial velocity V_0 of 56.1 km/h, a mean vehicle deceleration of 22.7 G. This condition represents an ideal frontal impact with total vehicle crumple length of 700mm. In order to examine the rate dependency on the thoracic response during the first segment of the input pulse, the authors applied three different values of t_c for the optimal pulses, which represent three ranks of the deflection rate of the spring element of the thorax. Here, they selected values of 20, 25 and 30 ms.

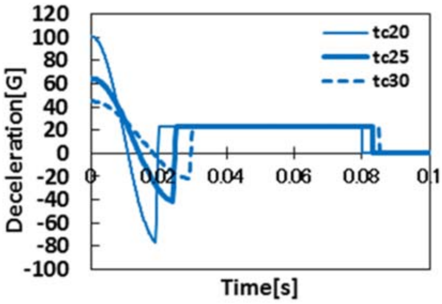

Fig. 8. Determined theoretical optimal pulses

Figure 8 indicates determined theoretical optimal pulses. These pulses were applied to the sled-buck model accommodating human and dummy models in the same manner as Phase 1 simulations.

III. RESULTS

Figures 9 to 12 indicate the results of the phase 1 simulations. Figure 9 indicates a comparison of the maximum values of thoracic deceleration under rectilinear input pulse with different magnitudes and with an identical duration. Figure 10 indicates those of the thoracic deflection. Figure 11 indicates a comparison of the maximum values of thoracic deceleration with rectilinear input pulses with an identical magnitude and different durations. Figure 12 indicates those of the thoracic deflection.

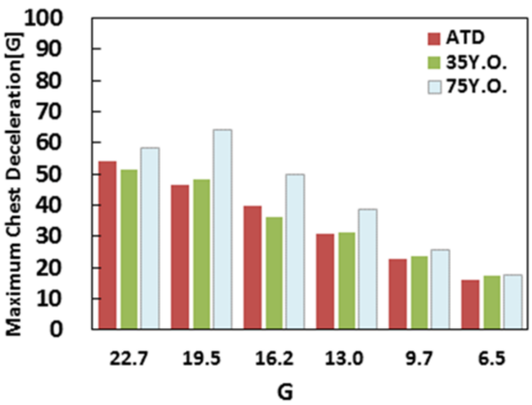

Fig. 9. Maximum thoracic deceleration with input pulses of different magnitudes with duration of 71 ms

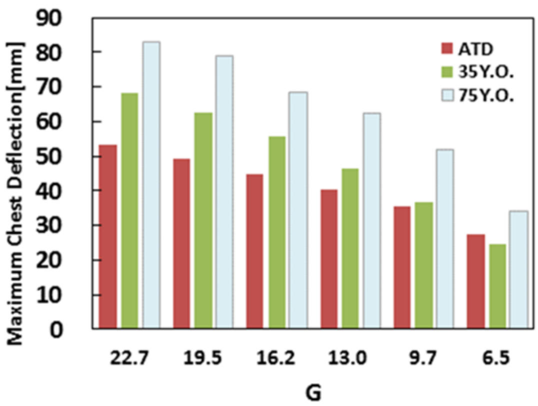

Fig. 10. Maximum thoracic deflection with input pulses of different magnitudes with duration of 71 ms

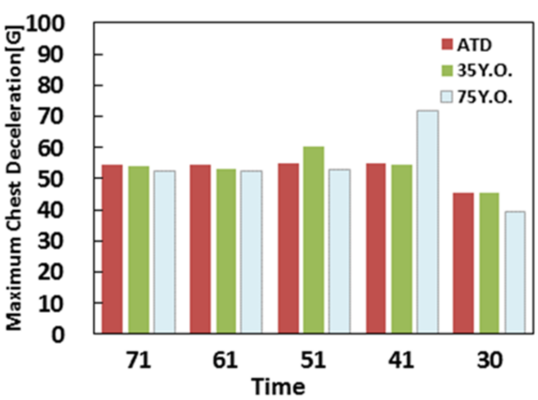

Fig. 11. Maximum thoracic deceleration with input pulses of 22.7 G with different durations

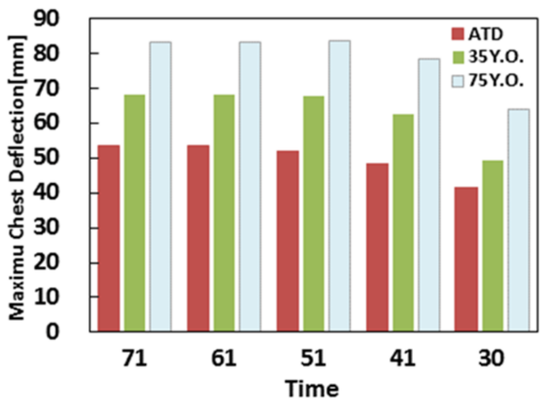

Fig. 12. Maximum thoracic deflection with input pulses of 22.7 G with different durations

Figures 13 to 18 indicate the results of the phase 2 simulations. Figure 13 indicates the pulses of the thoracic deceleration under the theoretical optimal pulses with t_c of 20 ms. Figure 14 indicates those of the thoracic deflection. Figures 15 and 16 indicate the respective pulses of the thoracic deceleration and deflection with t_c of 25 ms. Figures 17 and 18 indicate the respective pulses with t_c of 30 ms in the same manner.

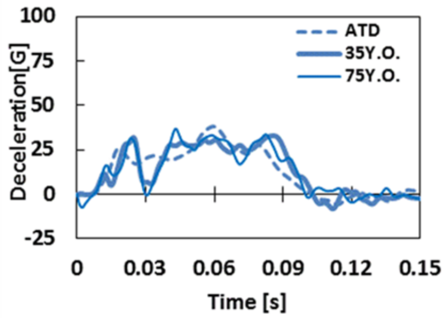

Fig. 13. Thoracic deceleration pulses for theoretical optimal pulse with t_c of 20 ms

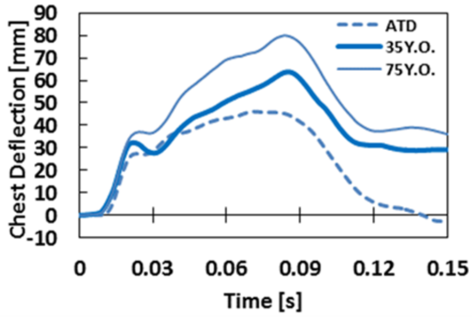

Fig. 14. Thoracic deflection pulses for theoretical optimal pulse with t_c of 20 ms

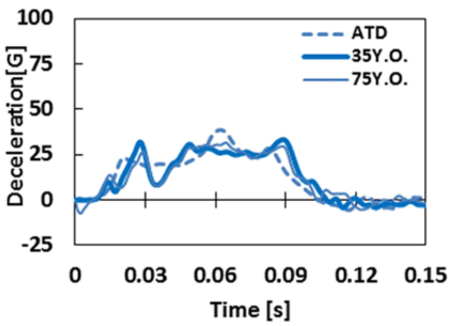

Fig. 15. Thoracic deceleration pulses for theoretical optimal pulse with t_c of 25 ms

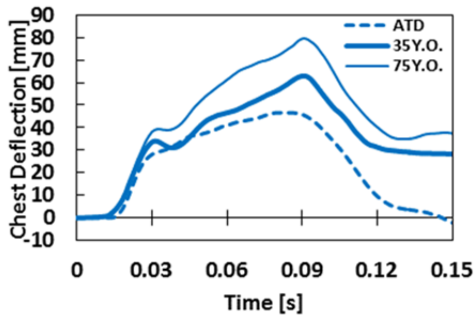

Fig. 16. Thoracic deflection pulses for theoretical optimal pulse with t_c of 25 ms

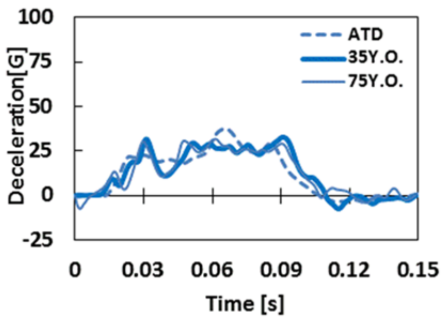

Fig. 17. Thoracic deceleration pulses for theoretical optimal pulse with t_c of 30 ms

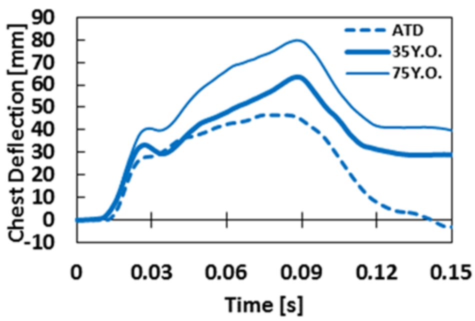

Fig. 18. Thoracic deflection pulses for theoretical optimal pulse with t_c of 30 ms

IV. DISCUSSION

As remarked above, the purpose of the present study is to examine the applicability of the theoretical optimal pulses to human occupants. However, the authors obtained several important findings from Phase 1 simulations.

In the first place, the authors discussed the response to the rectilinear pulses with an identical duration of 71ms and with different magnitudes. It was observed that the shapes of the pulses of the thoracic deflection indicate approximately haversine response during the onset both in the human models and the dummy model. And there was little difference in the rise time among each magnitude of input pulse. In other words, the effect of the rate dependency is not very dominant on the natural frequency of the system. On the other hand~~s~~, the peak value of the thoracic deflection increases with the magnitude of the pulse as well as deceleration (Figures 9, 10). The authors deem that these observations support the appropriateness of the simplification as a SDOF model when focusing on the onset of the thoracic deflection. Taking a look at the thoracic response to the rectilinear pulses with an identical magnitude, the maximum values of thoracic deceleration are almost identical among different durations (Figure 11), although the maximum values of thoracic deflection indicate slight increase with the increase of the duration of the applied pulse (Figure 12).

However, in the human models, the shapes of the thoracic deflection pulses indicate a longer trail from the rise time onwards as indicated in Figure 7, which suggests a certain kind of hysteresis. The values of the remaining (permanent) deflection after applying input pulses are larger in the elderly model than in the adult, and larger with pulses with higher magnitudes than with lower (Figures from 37 to 41 in Appendix).

Then, the authors looked at the strain contour chart of the adult human model, which indicates that the strain in the cortical bone of the ribs and the sternum reaches to above their yield strain at t=150 ms when applying a pulse with a magnitude of 22.7 G (Figure 19). Therefore, the authors deem this to be due to the plastic deformation of the rib cage.

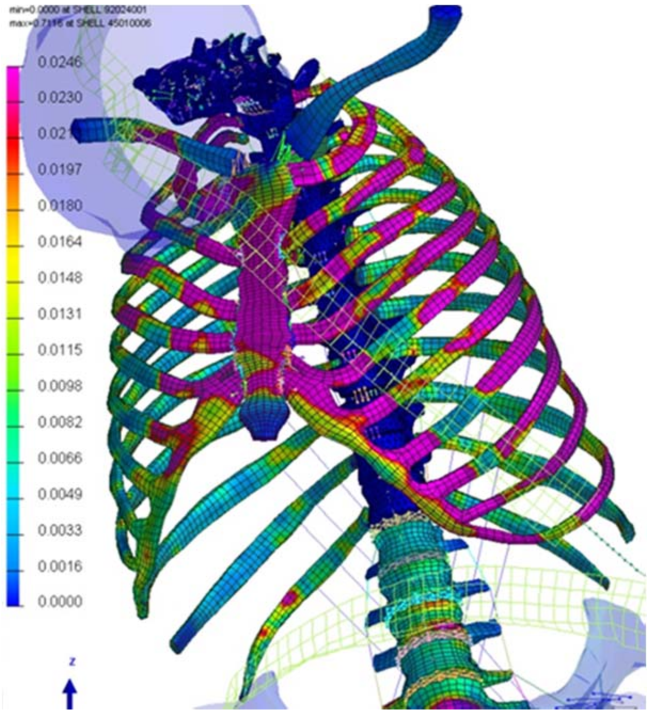

Fig. 19. Strain contour chart of adult human FE model with a 22.7 G rectilinear pulse at t=150 ms; strain on the ribs and sternum reaches more than 0.023, above yield strain

Next, the authors discussed the response to the theoretical optimal pulses. The authors applied three ranks of the deflection rate by applying theoretical optimal pulses with different respective t_c values of 20, 25 and 30 ms. However the response after t_c was almost identical among the pulses, showing trapezoid waveforms from t_c onwards. This supports the discussion regarding the rate dependency of the total spring coefficient based on the Phase 1 simulations.

On the contrary, with regard to the thoracic deflection, there was a significant difference between the dummy model and human models. In the dummy model the time history of the thoracic deflection indicated an approximate trapezoid waveform with a slight increase along the time axis, approximately tracing the response of the SDOF model [6-7]. However, in the human models, they indicated a linear increase along the time axis after their onset. A similar phenomenon to the response was observed in the dummy excursion when applying a seatbelt system with a load-limiter. This is deemed due to plastic deformation of the rib cage. Consequently, their maximum values approached values similar to those of responses with rectilinear pulses. Furthermore, the elderly model indicates the highest peak value among them. This suggests that the maximum values of the thoracic deflection in the human models are sensitive to the duration of the applied pulse if the strain in the cortical bone of the thorax exceeds its yield strain. The tendency when applying rectilinear pulses with different durations indicated in Figures 11 and 12 support this presumption. Therefore, these observations may suggest the necessity of theoretical optimization by applying a non-linear spring model with plastic deformation for the human model.

Limitations

The elderly model used in the present study has not yet been validated against the response from experimental results due to the lack of literature regarding whole body experiment using PMHS of age 75 Y/O or older.

In the human FE models used in the present study, element elimination option to represent bone fracture was not activated throughout the simulations. This was done to compare each fundamental whole body kinematics. Therefore, in the present study the authors did not discuss the post-fracture kinematics during high-energy impacts that might include non-continuous transition of the kinetic response due to immediate and catastrophic decrease of the thoracic stiffness after the occurrence of rib fracture.

V. CONCLUSIONS

The aim of the present study is to examine the applicability of the theoretical optimal pulses to the thoracic responses of the human occupants. The authors applied the theoretical optimal pulse as well as rectilinear pulse to the sled-buck model accommodating a human FE model. The human FE models used in the present study represent the anthropometry and material properties of 50th percentile American males of ages 35 Y/O and 75 Y/O. The thoracic responses of these models were analyzed. The results indicated the following findings. The response of the thoracic deceleration of the human FE model for the theoretical optimal pulse is almost identical to that of the dummy model. However, the response of the thoracic deflection of the human FE model after the onset differs from that of the dummy model, showing increase over time. The maximum values of the thoracic deflection are sensitive to the duration of the applied pulse in the human models. When applying the theoretical optimal pulses, the thoracic deflection indicated linear increase along the time axis after their onset. This is deemed due to plastic deformation of the rib cage. The elderly human FE model indicates larger thoracic deflection than that of the adult model. These observations suggest the limitation of the applicability of the theoretical optimal pulses as well as the necessity of theoretical optimization by applying an elastoplastic spring model.

VI. REFERENCES

[1] Zhou Q, Rouhana S, Melvin J, Age effects on thoracic injury tolerance, *Proceedings of Stapp Car Crash Conference,* paper number 962421, 1996.

[2] Kent R, Sherwood C, Shaw G, Lessley D, Overby B, Matsuoka F, Age related changes in the effective stiffness of the human thorax using four loading conditions, *Proceedings of IRCOBI Conference,* Isle of Man, 2001.

[3] Grimes WD, Lee FD, The effect of crash pulse shape on occupant simulations, paper number 2000-01-0460, *Society of Automotive Engineers*, Warrendale, Pennsylvania, 2000.

[4] Ishii K, Yamanaka I, Influence of vehicle deceleration curve on dummy injury criteria, paper number 880612, *Society of Automotive Engineers*, Warrendale, Pennsylvania, 1988.

[5] Takahashi K, Suzuki N, Sonoda Y, Komamura T, Suzuki T, Tawarayama T, Dokko Y, Optimization of vehicle deceleration curves for occupant injury, paper number 9307515, *Society of Automotive Engineers,* Warrendale, Pennsylvania, 1993.

[6] Motozawa Y, Kamei T, A new concept for occupant deceleration control in a crash, paper number 2000-01-0881, *Society of Automotive Engineers,* Warrendale, Pennsylvania, 2000.

[7] Motozawa Y, Tsuruta M, Kawamura Y, Noguchi J, A new concept for occupant deceleration control in a crash -Part 2, paper number 2003-01-1228, *Society of Automotive Engineers,* Warrendale, Pennsylvania, 2003.

[8] Wu J, Sukhbir S, Nusholts G, An impact pulse-restraint energy relationship and its applications, paper number 2003-01-0505, *Society of Automotive Engineers,* Warrendale, Pennsylvania, 2003.

[9] Ito O, Dokko Y, Ohhashi K, Development of human lower FE models of adult and elderly person considering aging effects. *Proceedings of JSAE Annual Congress (Spring),* Yokohama, Japan, paper number 20085048, 2008.

[10] Ito O, Dokko Y, Ohhashi K, Development of adult and elderly FE thorax skeletal models, paper number

2009-01-0381, doi:10.4271/ 2009-01-0381, *Society of Automotive Engineers,* Warrendale, Pennsylvania, 2009.

[11]Ito O, Dokko Y, Ohhashi K, Development of thorax skeletal FE models for adult and the elderly, *Transactions of JSAE, 40(6):1457-1467*, 2009.

[12]Dokko Y, Ito O, Kanayama Y, Ohhashi K, Development of human lumbar spine FE models for adult and the elderly, paper number 2009-01-0382, doi:10.4271/2009-01-0382, *Society of Automotive Engineers,* Warrendale, Pennsylvania, 2009.

[13]Dokko, Y, Ito O, Ohhashi K, Development of human lower limb and pelvis FE models for adult and the elderly, paper number 2009-01-0396, doi:10.4271/2009-01-0396, *Society of Automotive Engineers,* Warrendale, Pennsylvania, 2009.

[14]H-model™ Version 2007 User's Manual, *ESI Group*, 2007.

[15]Ruan JS, El-Jawahri R, Chai L, Barbat S, Prasad P, Prediction and analysis of human thoracic impact responses and injuries in cadaver impacts using a full human body finite element model, *Stapp Car Crash Journal,* 47:299-321, 2003.

[16]Yamada H, Strength of biological materials, *Lippincott Williams & Wilkins,* Baltimore, MD. 13-978-0683093230, 1970.

[17]Kroell C, Schneider D, Nahum A, Impact tolerance and response of the human thorax, paper number 710851, *Society of Automotive Engineers,* Warrendale, Pennsylvania, 1971.

[18]Kroell C, Schneider D, Nahum A, Impact tolerance and response of the human thorax II, paper number 741187, *Society of Automotive Engineers,* Warrendale, Pennsylvania, 1974.

[19]Lessley DJ, Salzar R, Crandall J, Kent R, Bolton JR, Bass CR, Forma JL, Kinematics of the thorax under dynamic belt loading conditions, *International Journal of Crashworthiness,* 15(2):175-190, 2010.

[20]Ito Y, Dokko Y, Mori F, Motozawa Y, Ohhashi K, Kinematics validation of age-specific restrained 50th percentile occupant FE models in frontal impact, paper number 2012-01-0565, doi:10.4271/2012-01-0565, *Society of Automotive Engineers,* Warrendale, Pennsylvania, 2012.

[21]Rhule HH, Maltese MR, Donnelly BR, Eppinger RH, Brunner JK, Bolte JH IV, Development of a new biofidelity ranking system for anthropomorphic test devices, *Stapp Car Crash Journal,* 46:477-512, 2002.

VII. APPENDIX

All figures shown in this chapter indicate the results of the phase 1 simulations.

Figures 20 to 25 indicate the thoracic deceleration pulses under rectilinear pulse with different magnitudes and with an identical duration of 71 ms. Figures 26 to 31 indicate those of the thoracic deflection.

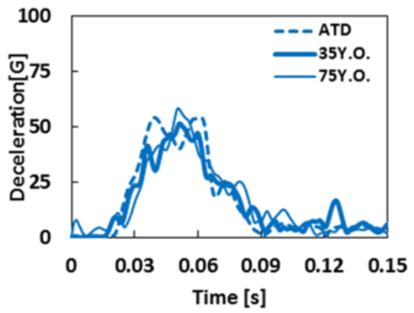

Fig. 20. Thoracic deceleration pulses; Input pulse 22.7 G / 71 ms

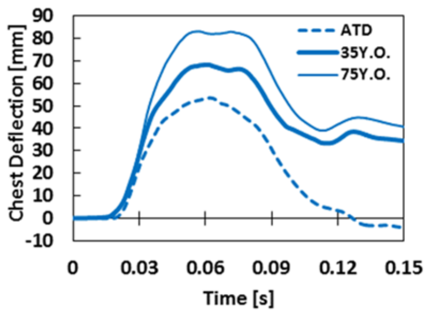

Fig. 26. Thoracic deflection pulses; Input pulse 22.7 G / 71 ms

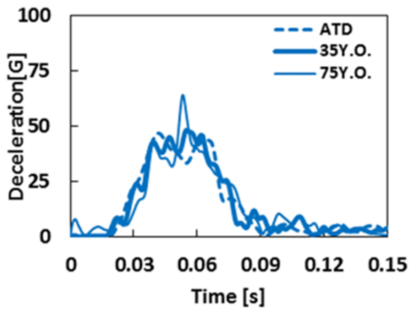

Fig. 21. Thoracic deceleration pulses; Input pulse 19.5 G / 71 ms

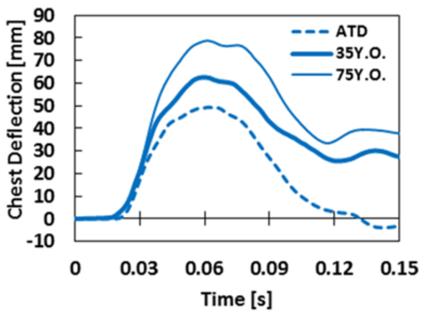

Fig. 27. Thoracic deflection pulses; Input pulse 19.5 G / 71 ms

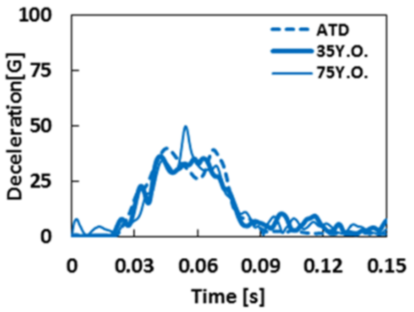

Fig. 22. Thoracic deceleration pulses; Input pulse 16.2 G / 71 ms

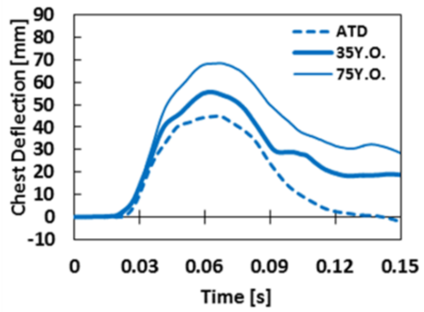

Fig. 28. Thoracic deflection pulses; Input pulse 16.2 G / 71 ms

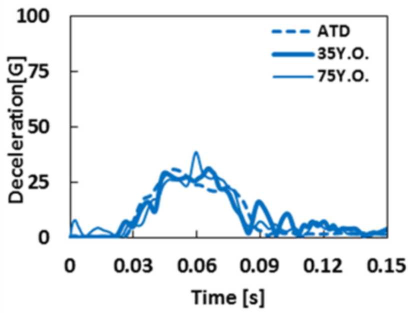

Fig. 23. Thoracic deceleration pulses; Input pulse 13.0 G / 71 ms

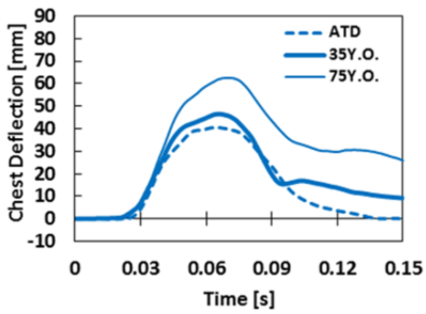

Fig. 29. Thoracic deflection pulses; Input pulse 13.0 G / 71 ms

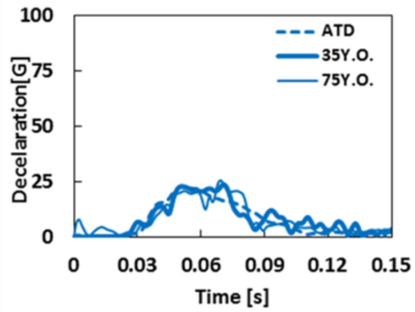

Fig. 24. Thoracic deceleration pulses; Input pulse 9.73 G / 71 ms

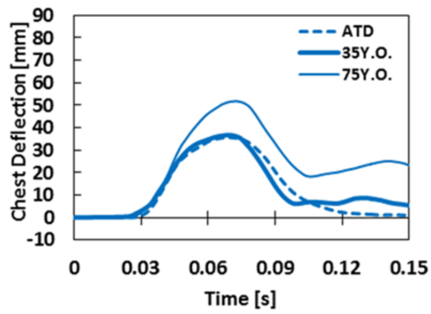

Fig. 30. Thoracic deflection pulses; Input pulse 9.73 G / 71 ms

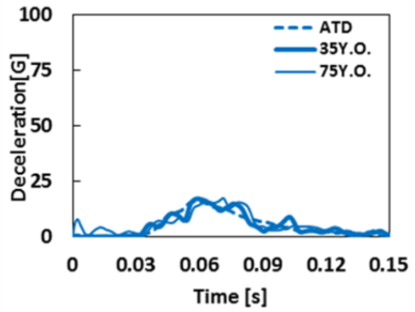

Fig. 25. Thoracic deceleration pulses; Input pulse 6.49 G / 71 ms.

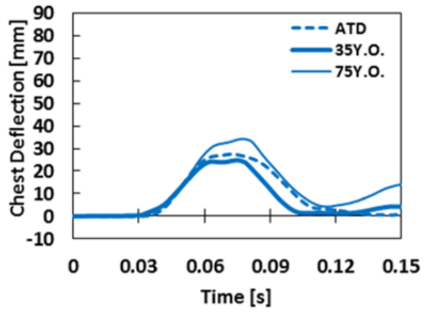

Fig. 31. Thoracic deflection pulses; Input pulse 6.49 G / 71 ms

Figures from 32 to 36 indicate the thoracic deceleration pulses under rectilinear pulses with an identical magnitude of 22.7G and with different durations. Figures from 37 to 41 indicate those of the thoracic deflection.

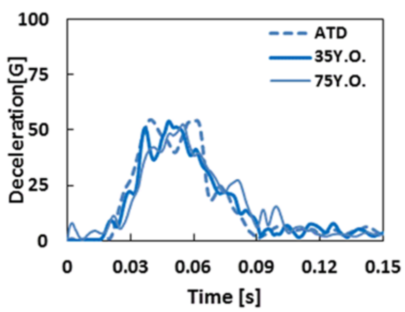

Fig. 32. Thoracic deceleration pulses; Input pulse 22.7 G / 71 ms

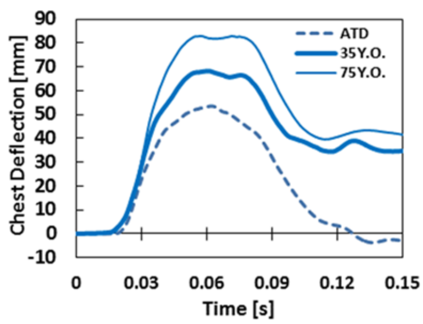

Fig. 37. Thoracic deflection pulses; Input pulse 22.7 G / 71 ms

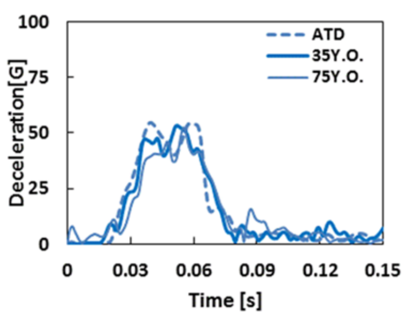

Fig. 33. Thoracic deceleration pulses; Input pulse 22.7G / 61 ms

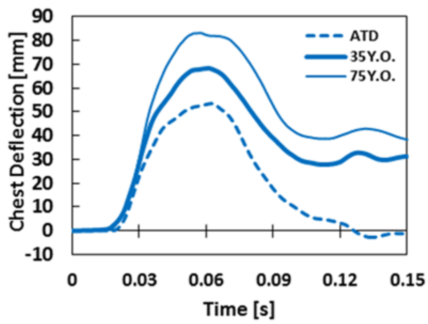

Fig. 38. Thoracic deflection pulses; Input pulse 22.7 G / 61 ms

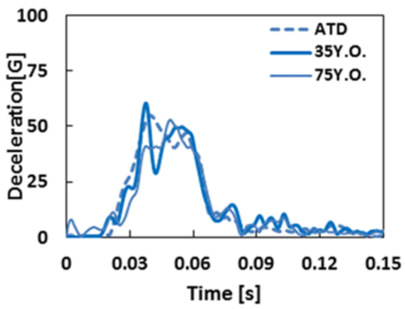

Fig. 34. Thoracic deceleration pulses; Input pulse 22.7G / 51 ms

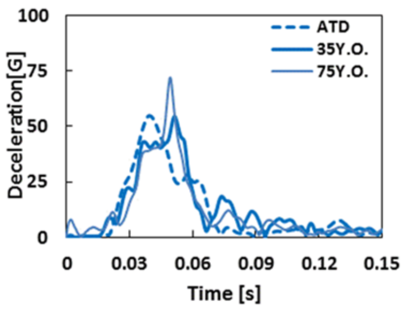

Fig. 35. Thoracic deceleration pulses; Input pulse 22.7G / 41 ms

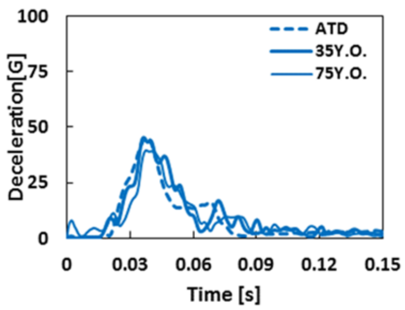

Fig. 36. Thoracic deceleration pulses; Input pulse 22.7G / 31 ms

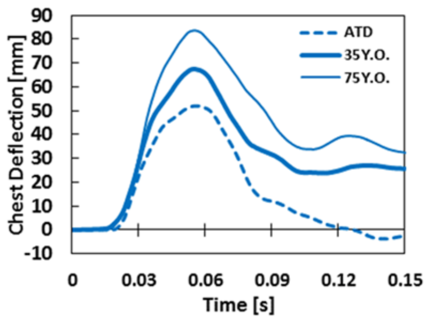

Fig. 39. Thoracic deflection pulses; Input pulse 22.7 G / 51 ms

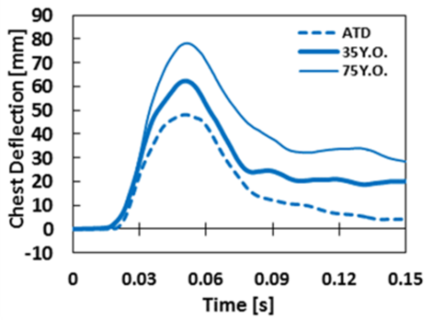

Fig. 40. Thoracic deflection pulses; Input pulse 22.7 G / 41 ms

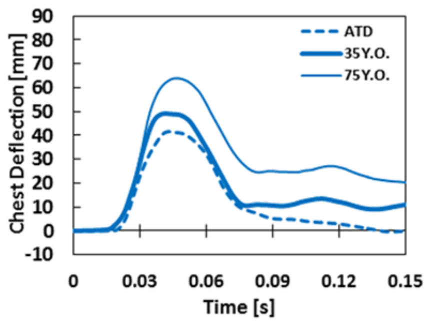

Fig. 41. Thoracic deflection pulses; Input pulse 22.7 G / 31 ms